Li, X., Ge, M., Zhang, H., Wang, R., Guo, B., Klotz, J., Wickert, J., Schuh, H. (2013): High-Rate coseismic displacements from tightly integrated processing of raw GPS and accelerometer data. - Geophysical Journal International, 195, 1, pp. 612—624.

DOI: http://doi.org/10.1093/gji/ggt249

Geophysical Journal International

Geophys. J. Int. (2013) **195,** 612–624
Advance Access publication 2013 July 18

doi: 10.1093/gji/ggt249

High-rate coseismic displacements from tightly integrated processing of raw GPS and accelerometer data

Xingxing Li,[1,2] Maorong Ge,[1] Yong Zhang,[1,3] Rongjiang Wang,[1] Bofeng Guo,[2] Jürgen Klotz,[1] Jens Wickert[1] and Harald Schuh[1]

[1] *German Research Centre for Geosciences (GFZ), Telegrafenberg,* 14473 *Potsdam, Germany. E-mail: lixin@gfz-potsdam.de*
[2] *School of Geodesy and Geomatics, Wuhan University,* 129 *Luoyu Road,* 430079*, Wuhan, Hubei, China*
[3] *Institute of Geophysics, China Earthquake Administration, No.* 5 *Minzudaxue Nanlu, Beijing* 100081*, China*

Accepted 2013 June 19. Received 2013 June 19; in original form 2013 January 11

SUMMARY

High-rate GPS and seismic sensors are mutually contributing to seismological applications for capturing earthquake-induced coseismic displacements. In this study, we propose an approach for tightly integrating GPS and strong motion data on raw observation level to increase the quality of the derived displacements. The performance of the proposed approach is demonstrated using 5 Hz high-rate GPS and 200 Hz strong motion data collected during the El Mayor–Cucapah earthquake (M_w 7.2, 2010 April 4) in Baja California, Mexico. The new approach not only takes advantages of both GPS and strong motion sensors, but also improves the reliability of the displacement by enhancing GPS integer-cycle phase ambiguity resolution, which is very critical for deriving displacements with highest quality.

Key words: Satellite geodesy; Transient deformation; Earthquake ground motions; Early warning.

1 INTRODUCTION

Since Remondi (1985) first demonstrated centimetre-level accuracy of kinematic GPS, Hirahara *et al.* (1994) labelled kinematic GPS as GPS seismology, which has since attracted more and more attention and applications in seismology (see, e.g. Ge 1999; Ge *et al.* 2000; Larson 2009). High-rate GPS observes displacements directly and thus particularly valuable in case of large earthquakes (Nikolaidis *et al.* 2001; Larson *et al.* 2003; Allen & Ziv 2011). In recent years, dense GPS monitoring networks have proliferated in seismically active regions, for example, Japan's GEONET [the GPS Earth Observation Network System, http://www.gsi.go.jp/ (last accessed July 2013)] and UNAVCO's Plate Boundary Observatory [PBO, http://pbo.unavco.org/ (last accessed July 2013)], which have the potential to be complementary to seismic networks and may contribute to earthquake/tsunami early warning and seismic risk mitigation (Blewitt *et al.* 2006, 2009; Crowell *et al.* 2009).

The problem with GPS displacement is that its noise level is much higher than that from most seismic sensors. In GPS displacements, this noise is basically white across the whole seismic frequency band. Seismic sensors measure acceleration with a very high precision and sampling rate and the seismic displacements can be obtained by double integration of the observed accelerometer signals. However, the acceleration is accompanied by unphysical drifts due to sensor rotation and tilt (Trifunac & Todorovska 2001; Lee & Trifunac 2009), hysteresis (Shakal & Petersen 2001) and imprecision in the numerical integration process (Boore *et al.* 2002; Smyth & Wu 2006). Its noise level, viewed in terms of displacement, will rise with decreasing frequency: at some frequency this noise level will exceed that of GPS. Therefore, GPS and seismic instruments can be mutually beneficial for seismological applications because weaknesses of one observation technique are offset by strengths in the other.

To take full use of the complementary of GPS and seismic sensors, we propose an approach of integrating the accelerometer data into the precise point positioning (PPP, Zumberge *et al.* 1997) processing. Instead of combing the GPS-derived displacements with the accelerometer data (Emore *et al.* 2007; Bock *et al.* 2011), a tightly integrated filter is developed to estimate seismic displacements from GPS phase and range and accelerometer observations. The performance of the proposed tightly integrated approach was validated by the 2010, M_w 7.2 El Mayor–Cucapah earthquake (M_w 7.2, 2010 April 4) in Baja California, Mexico.

2 OVERVIEW OF COMBINING GPS AND ACCELEROMETER DATA

GPS relative kinematic positioning is usually adopted to estimate seismic displacements as double-differenced ambiguities can be fixed to integers for guaranteeing high accuracy (Larson *et al.*

Table 1. Collocated high-rate GPS and strong motion (SM) stations.

Station (GPS/SM)	Latitude (°N)	Longitude (°W)	Distance to epicentre (km)	Separation (km)
P500	32.690	−115.300	48.4	0.56
NP5054	32.693	−115.338		
P496	32.751	−115.596	61.8	0.07
NP5058	32.752	−115.595		
P744	32.829	−115.508	66.4	0.14
NP5028	32.829	−115.505		
P499	32.980	−115.488	83.9	1.80
NP5060	32.991	−115.513		

2003; Blewitt *et al.* 2006; Crowell *et al.* 2012; Melgar *et al.* 2012; Ohta *et al.* 2012). In relative positioning, data from a network are analysed simultaneously to estimate station positions with respect to at least one reference station which could also be displaced. PPP can provide 'absolute' seismic displacements related to a global reference frame defined by the satellite orbits and clocks with a single GPS receiver (Kouba 2003; Wright *et al.* 2012). Especially, PPP integer ambiguity resolution, developed in recent years (Ge *et al.* 2008; Geng *et al.* 2012; Li & Zhang 2012; Loyer *et al.* 2012), enables it to achieve comparable accuracy as relative positioning. Li *et al.* (2013a) demonstrated the performance of real-time PPP with ambiguity resolution using 5 Hz GPS data collected during El Mayor–Cucapah earthquake (M_w 7.2, 2010 April 4) in Mexico.

Emore *et al.* (2007) estimated GPS displacements based on relative network analysis using the GPS analysis software GIPSY, developed by JPL (Jet Propulsion Laboratory) with orbits held fixed to precise IGS (International GNSS Service) final products. A constrained inversion technique was then used to combine GPS displacements and accelerometer data from the 2003 M_w 8.3 Tokachi-oki earthquake to estimate displacements and step function offsets in accelerometer records, after correcting for possible misorientation of the accelerometers.

A multirate Kalman filter was proposed by Smyth & Wu (2006) for fusing raw accelerometer with collocated GPS displacement data and was used for bridge monitoring (Kogan *et al.* 2008) and structural engineering applications (Chan *et al.* 2006). Bock *et al.* (2011) applied the multirate Kalman filter to estimate broad-band displacements for the 2010 M_w 7.2 El Mayor–Cucapah earthquake by combining 1 Hz GPS displacements and 100 Hz data of collocated strong motion sensor in southern California. Hereby the 1 Hz GPS displacement was estimated using instantaneous GPS positioning in relative positioning mode (Bock *et al.* 2000). Geng *et al.* (2013) proposed a seismogeodetic approach and applied it to GPS and accelerometer observations of the 2012 Brawley seismic swarm. Melgar *et al.* (2013) demonstrated the Kalman filter performance for the Tohoku-oki event and analysed the spectral differences between GPS, Kalman and accelerometer data in detail. Wang *et al.* (2013) discussed the potential for an automated baseline correction scheme for accelerometer data that does not rely on GPS data.

In these combination procedures, the long-period stability of GPS-derived positions is employed to constrain the seismic data. As is well known, in kinematic positioning, precise dynamical information will give rather tight constraint on coordinates of adjacent epochs to strengthen the solution for more reliable ambiguity fixing and better displacement accuracy. The precise dynamical information of the movement provided by seismic sensors cannot be properly utilized to enhance GPS solutions if estimated coordinates are used. Therefore, integration on the observation level is required to have the advantages of both sensors and offset their weakness. In this study, the accelerometer data are integrated into the ambiguity-fixed PPP processing on the raw observation level.

3 THE TIGHTLY INTEGRATED ALGORITHM

Fixing ambiguities to integers can significantly improve the GPS positioning quality, especially for the east component (e.g. Blewitt 1989; Dong & Bock 1989). Due to the existence of uncalibrated phase delays (UPDs) originating at receiver and satellite (Blewitt 1989), for a long time only double-differenced ambiguities between satellites and receivers can be fixed. In the recent years, it was demonstrated that satellite UPDs could be estimated from a reference network and applied to other stations for fixing integer ambiguity in PPP mode (Collins *et al.* 2008; Ge *et al.* 2008; Laurichesse *et al.* 2008; Li *et al.* 2013b). Thus, PPP with integer ambiguity fixing requires not only precise satellite orbit and high-rate satellite clock corrections but also UPDs product. There are several IGS real-time analysis centres providing UPDs product for PPP ambiguity fixing (Ge *et al.* 2012; Loyer *et al.* 2012). With the corrections of GPS satellite orbits, clocks and UPDs, the corresponding biases in the observations can be removed. The receiver-dependent UPD can be assimilated into receiver clock parameter. Hence, the linearized equations for raw carrier phase and pseudo-range observations then can be simplified as (Teunissen & Kleusberg 1996)

$$l_j^s = -u^s \cdot \Delta r + m^s \cdot Z + t - I_j^s + \lambda_j N_j^s + \varepsilon_j^s, \tag{1}$$

$$p_j^s = -u^s \cdot \Delta r + m^s \cdot Z + t + I_j^s + e_j^s, \tag{2}$$

where, l_j^s and p_j^s denote 'observed minus computed' phase and code observables from satellite s to receiver at frequency j; u^s is the unit direction vector from receiver to satellite; Δr denotes the vector of the receiver positions; Z denotes tropospheric zenith wet delay; m^s is the wet part of global mapping function; t are the receiver clock errors; λ_j is the wavelength of the j frequency; I_j^s is ionospheric delay on the path at the j frequency; N_j^s is the integer phase ambiguity; e_j^s is the pseudo-range measurement noise; ε_j^s is measurement noise of carrier phase. Other error components such as the dry tropospheric delay, phase centre offsets and variations, phase wind-up, relativistic effect and tide loading could be corrected with existing models (Kouba & Héroux 2001).

Usually the ionosphere-free linear combination is employed in PPP to eliminate the effect of ionospheric delays. To suppress the measurement noise, instead of such linear combination we use in this contribution raw carrier-phase and pseudo-range observations at L1 and L2 frequencies (Schaffrin & Bock 1988). The slant ionospheric delays are estimated as unknown parameters and a temporal constraint is introduced to strengthen the solution. Assuming that n satellites are observed by the receiver at the epoch k, the observational equations for all the satellites at this epoch can be expressed as,

$$Y_k = A_k \cdot X_k + \varepsilon_{Y_k}, \varepsilon_Y \sim N(0, Q_Y), \tag{3}$$

$$Y = \begin{pmatrix} \left(L_1^T, L_2^T\right)^T \\ \left(P_1^T, P_2^T\right)^T \end{pmatrix}, L_j = \left(l_j^1, \cdots, l_j^n\right)^T, P_j = \left(p_j^1, \cdots, p_j^n\right)^T. \tag{4}$$

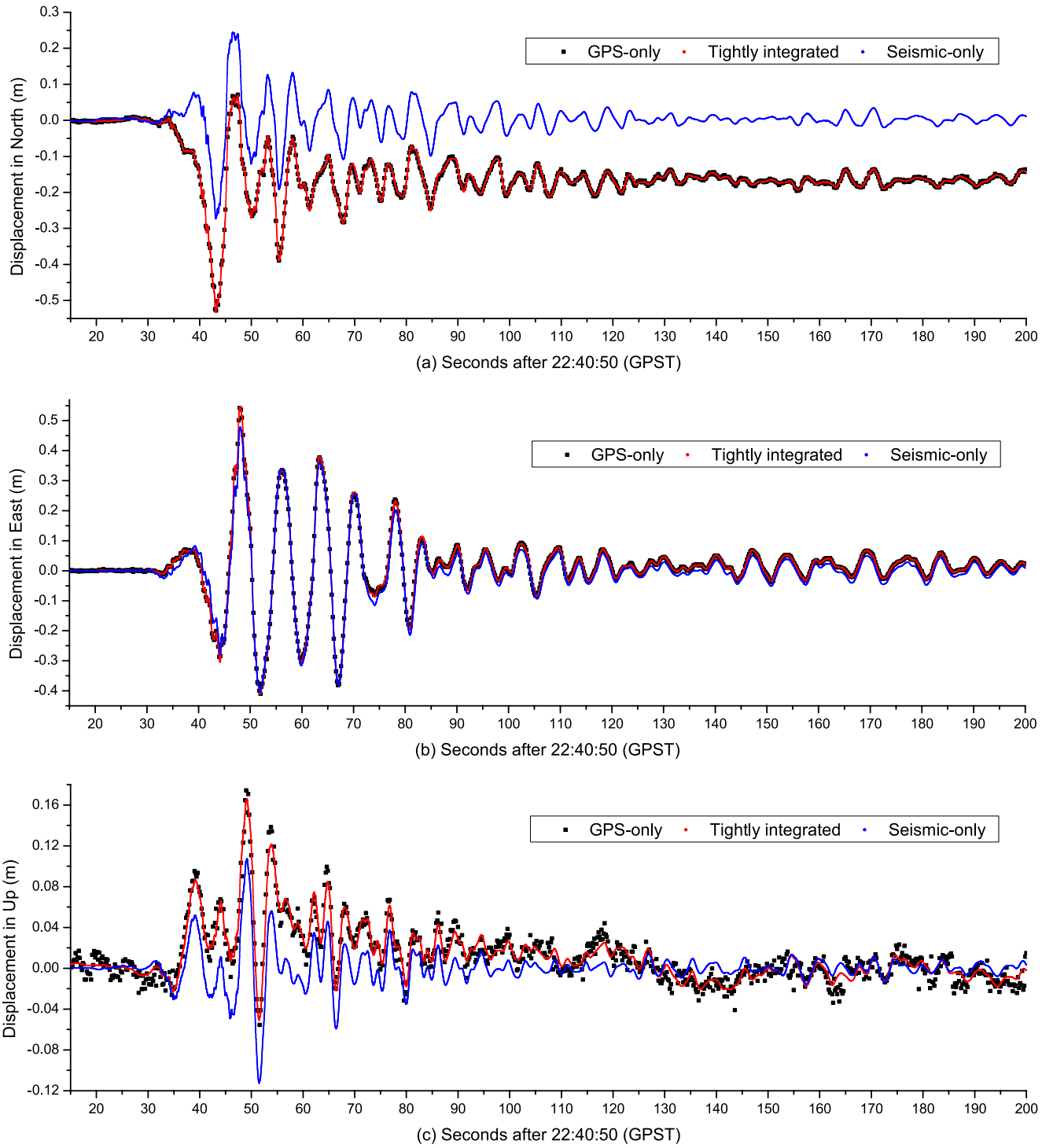

Figure 1. Comparison of GPS-only, seismic-only and tightly integrated displacements on the collocated 5058 (seismic) and P496 (GPS) stations during the El Mayor–Cucapah earthquake on 2010 April 4. The subparts (a)–(c) show the entire period of seismic shaking in north, east and up components, respectively. The 5 Hz GPS-only, 200 Hz seismic-only, and 200 Hz tightly integrated displacements are, respectively, shown by the black, blue and red lines.

The design matrix and unknown parameters are:

$$A = \left(\begin{pmatrix} j_2 \\ j_2 \end{pmatrix} \otimes A', \begin{pmatrix} j_2 \\ j_2 \end{pmatrix} \otimes j_n, \begin{pmatrix} -\kappa \\ \kappa \end{pmatrix} \otimes J_n, \begin{pmatrix} \lambda \\ 0_2 \end{pmatrix} \otimes J_n \right), \quad (5)$$

$$A' = \begin{pmatrix} -u^1 & 0 & m^1 \\ \vdots & \vdots & \vdots \\ -u^n & 0 & m^n \end{pmatrix}, \kappa = \begin{pmatrix} 1 \\ \lambda_2^2/\lambda_1^2 \end{pmatrix}, \lambda = \begin{pmatrix} \lambda_1 & 0 \\ 0 & \lambda_2 \end{pmatrix}, \quad (6)$$

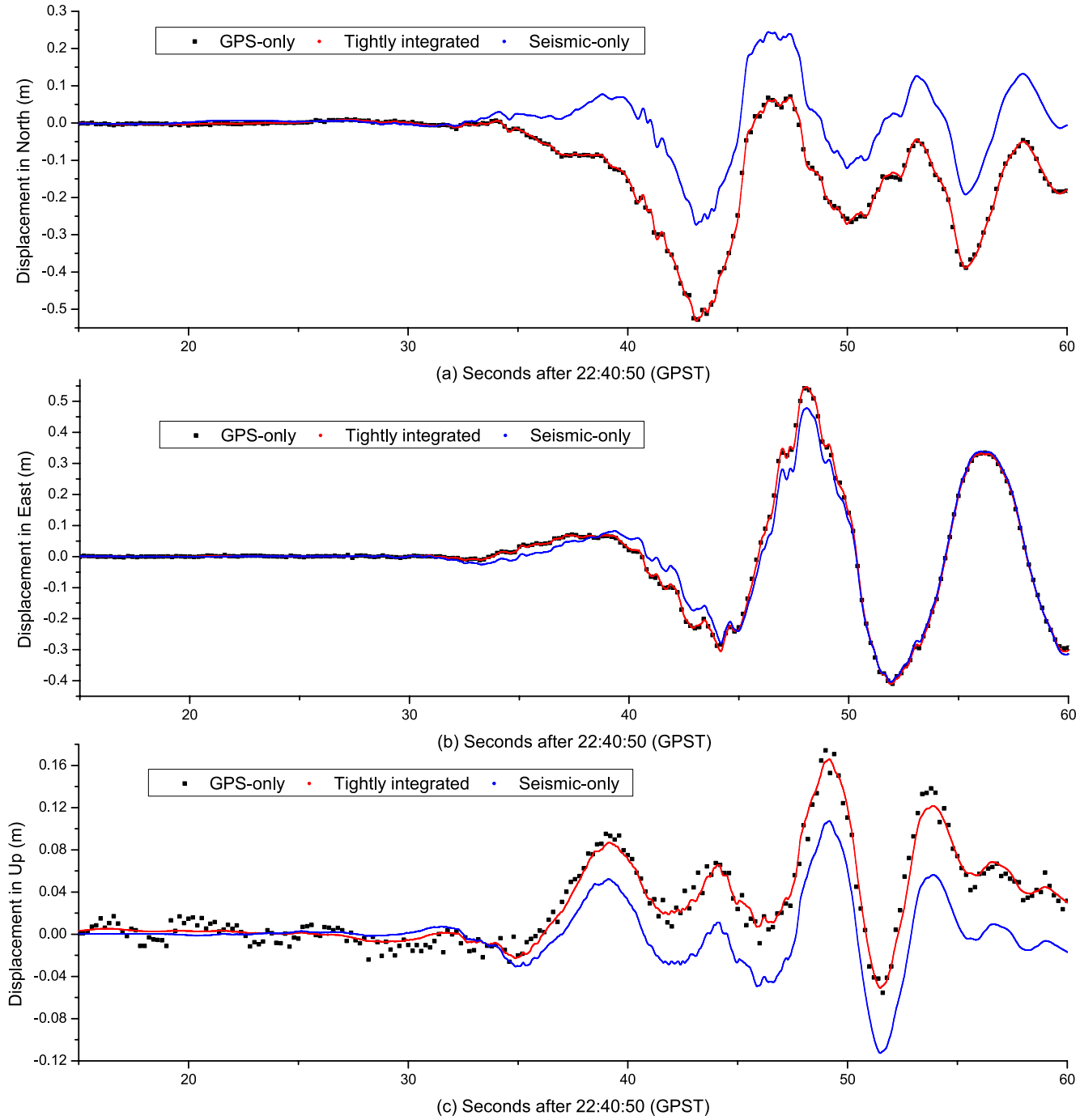

Figure 2. The blowup of the first 45 s of the coseismic displacements in all three components on the collocated 5058 (seismic) and P496 (GPS) stations during the El Mayor–Cucapah earthquake on 2010 April 4. The north, east and up components are shown in the subparts (a)–(c), respectively.

$$X = \left(\Delta r^T \Delta \dot{r}^T Zt(I_1^s)^T (N_1^s)^{\mathrm{T}} (N_2^s)^T\right)^T, (s = 1, \cdots, n), \tag{7}$$

where $\Delta\dot{r}$ denotes the vector of the receiver velocity; J_n is an identity matrix of n dimension; j_n denotes a column vector of n dimension in which all of the elements are unity; $\otimes$ is the Kronecker product; Q_Y is the variance–covariance matrix of ε_Y; κ is the coefficient of ionospheric delay.

The state equation can be described by:

$$X_k = \Phi_{k-1} \cdot X_{k-1} + \psi_{k-1} \cdot a_{k-1} + \varepsilon_{Sk-1}, \varepsilon_S \sim N(0, Q_S), \tag{8}$$

$$\Phi = \begin{pmatrix} J_3 & \tau \cdot J_3 & & & \\ & J_3 & & & \\ & & 1 & & \\ & & & 0 & \\ & & & & J_n \\ & & & & & J_{2n} \end{pmatrix}, \psi = \begin{pmatrix} \frac{\tau^2}{2} \cdot J_3 \\ \tau \cdot J_3 \\ 0_{1*3} \\ 0_{1*3} \\ 0_{n*3} \\ 0_{2n*3} \end{pmatrix}, \tag{9}$$

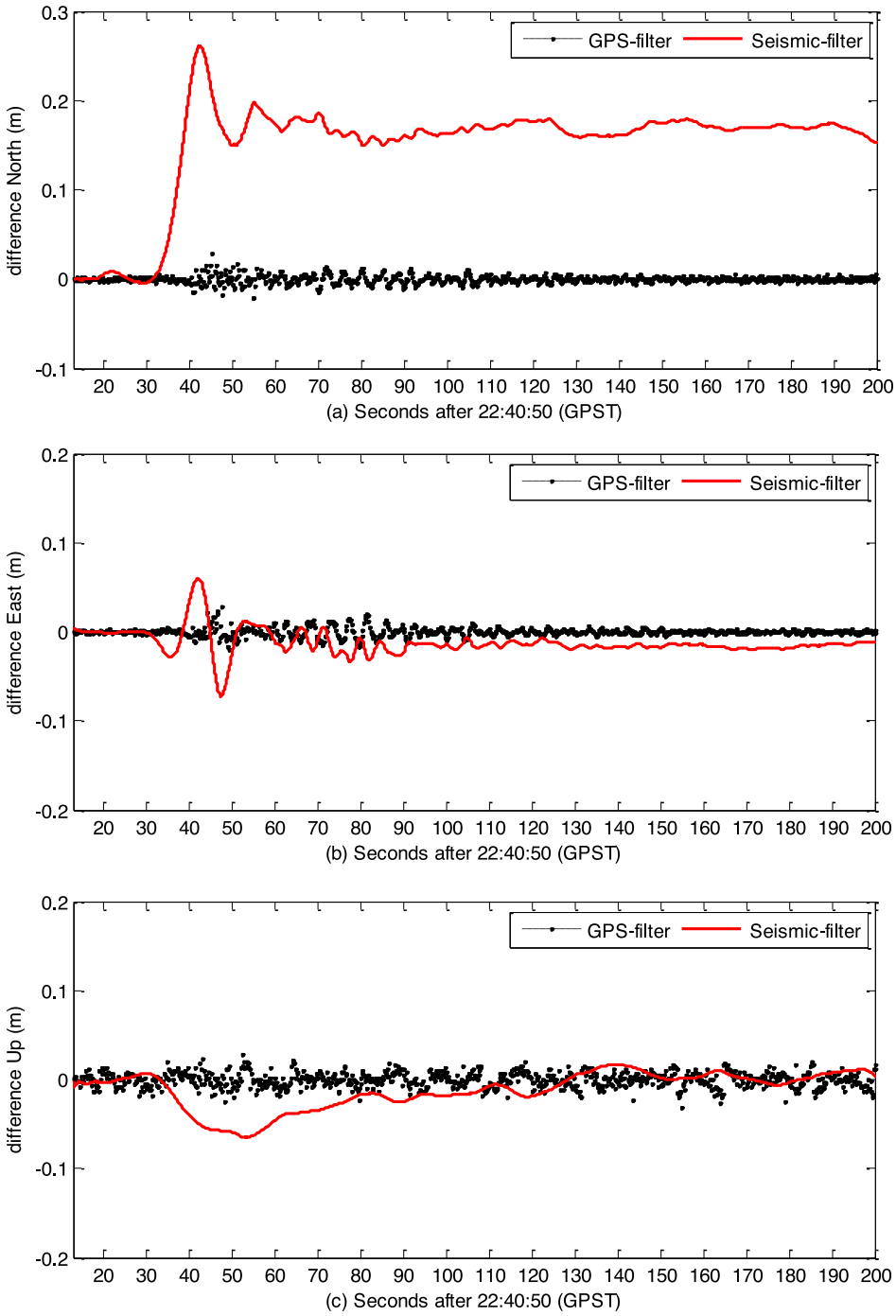

Figure 3. Difference between the displacement series from tightly integrated filter and each of the two inputs (GPS and seismic displacements) for 5058/P496 pair. The differences between GPS-only and filter displacements are shown by the black line, while the differences between seismic-only and filter displacements are shown by the red line. The differences in north, east and up components are, respectively, shown in the subparts (a)–(c).

$$Q_s = \begin{pmatrix} \frac{\tau^3}{3}\cdot q_a & \frac{\tau^2}{2}\cdot q_a & & & & & \\ \frac{\tau^2}{2}\cdot q_a & \tau\cdot q_a & & & & & \\ & & \tau\cdot q_z & & & & \\ & & & \tau\cdot q_t & & & \\ & & & & \tau\cdot q_i & & \\ & & & & & 0_{2n} & \end{pmatrix}, \quad (10)$$

where, Φ is the system dynamics matrix; a is the system inputs vector (raw accelerometer observations from the seismic sensor); Ψ is the input matrix; τ is the accelerometer sampling interval; Q_S is the variance–covariance matrix of ε_S; q_a is the acceleration variance (1000 times the pre-event noise of 60 s in this paper); q_z, q_t and q_i are the variances for the zenith wet delay (about 2–5mm$\sqrt{\text{hour}^{-1}}$), receiver clock (is set to white noise with a very large value) and ionospheric delay (generally a few millimetres for the 5 Hz data sampling), respectively.

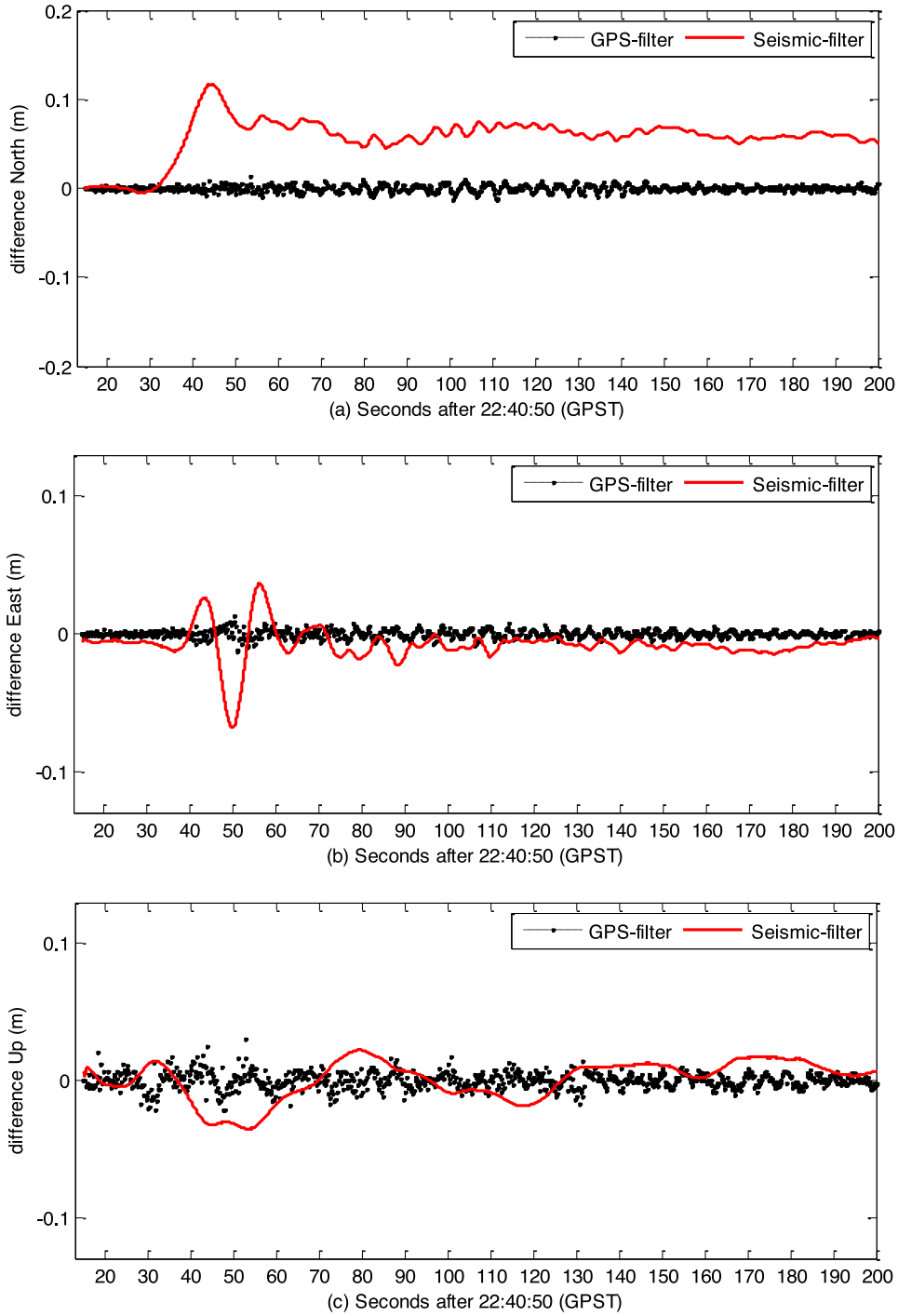

Figure 4. Difference between the displacement series from tightly integrated filter and each of the two inputs (GPS and seismic displacements) for 5028/P744 pair. The differences between GPS-only and filter displacements are shown by the black line, while the differences between seismic-only and filter displacements are shown by the red line. The differences in north, east and up components are, respectively, shown in the subparts (a)–(c).

With the GPS observational equations of (3) and the state equations of (8), the real-time Kalman filter can be employed to estimate the unknown parameters,

$$\bar{X}_k = \Phi_{k-1} \cdot \hat{X}_{k-1} + \psi_{k-1} \cdot a_{k-1}, \tag{11}$$

$$\bar{Q}_k = \Phi_{k-1} \cdot Q_{k-1} \cdot \Phi_{k-1}^T + Q_{S_{k-1}}, \tag{12}$$

$$\hat{X}_k = \bar{X}_k + Q_k A_k^T Q_{Y_k}^{-1} \cdot (Y_k - A_k \cdot \bar{X}_k), \tag{13}$$

$$Q_k = \left(\bar{Q}_k^{-1} + A_k^T \cdot Q_{Y_k}^{-1} \cdot A_k\right)^{-1}, \tag{14}$$

The time update of (11) and (12) is performed at every accelerometer sampling, while the measurement update of (13) and (14) is applied at every GPS epoch. The time and particularly the frequency domain performance of the filter can also be improved in post-processing with a smoother and in near real-time with a fixed lag smoother (Bock *et al.* 2011; Melgar *et al.* 2013).

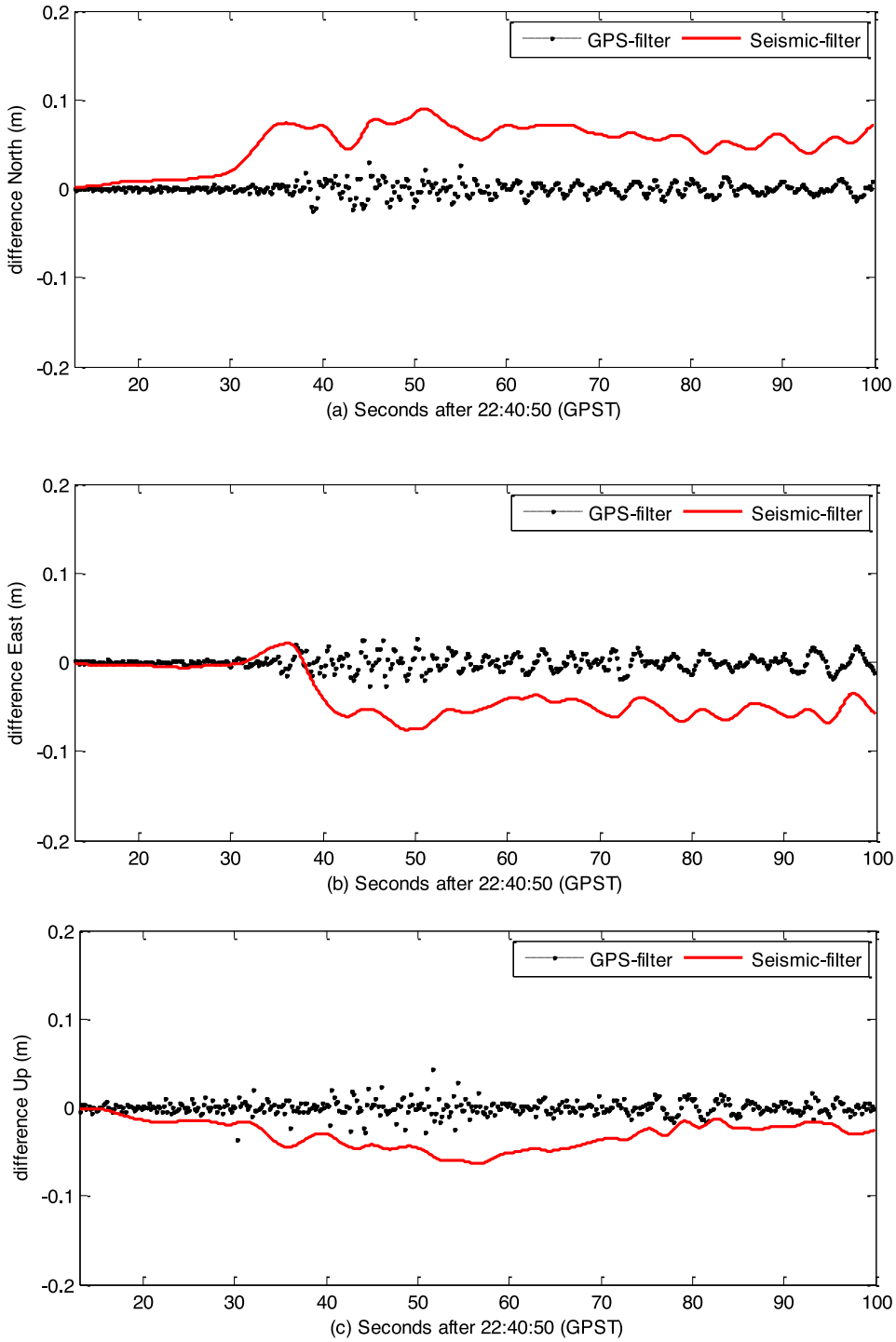

Figure 5. Difference between the displacement series from tightly integrated filter and each of the two inputs (GPS and seismic displacements) for 5054/P500 pair. The differences between GPS-only and filter displacements are shown by the black line, while the differences between seismic-only and filter displacements are shown by the red line. The differences in north, east and up components are, respectively, shown in the subparts (a)–(c).

The integer ambiguity resolution is attempted at every GPS epoch, L1 and L2 ambiguities are fixed simultaneously using the LAMBDA method by Teunissen (1995). With the predicted ionospheric delays from previous ambiguity-fixed epochs, reliable ambiguity resolution is achievable within few seconds for re-convergence (e.g. Geng *et al.* 2010; Zhang & Li 2012; Li *et al.* 2013b), although a convergence period of about 20 min for ambiguity fixing is still required.

Another critical issue is the validation of the fixed integer ambiguities. There are several approaches to assess the resolved integer ambiguities, such as *R*-ratio, *W*-ratio as well as the Integer Aperture-based *R*-ratio, and *W*-ratio methods (Li & Wang 2012). In this study, the well-known *R*-ratio test was used to validate the ambiguity resolution. The *R*-ratio is defined as the proportion of the second minimum and the minimum quadratic distances between the integer and the real-valued ambiguities. It is used to

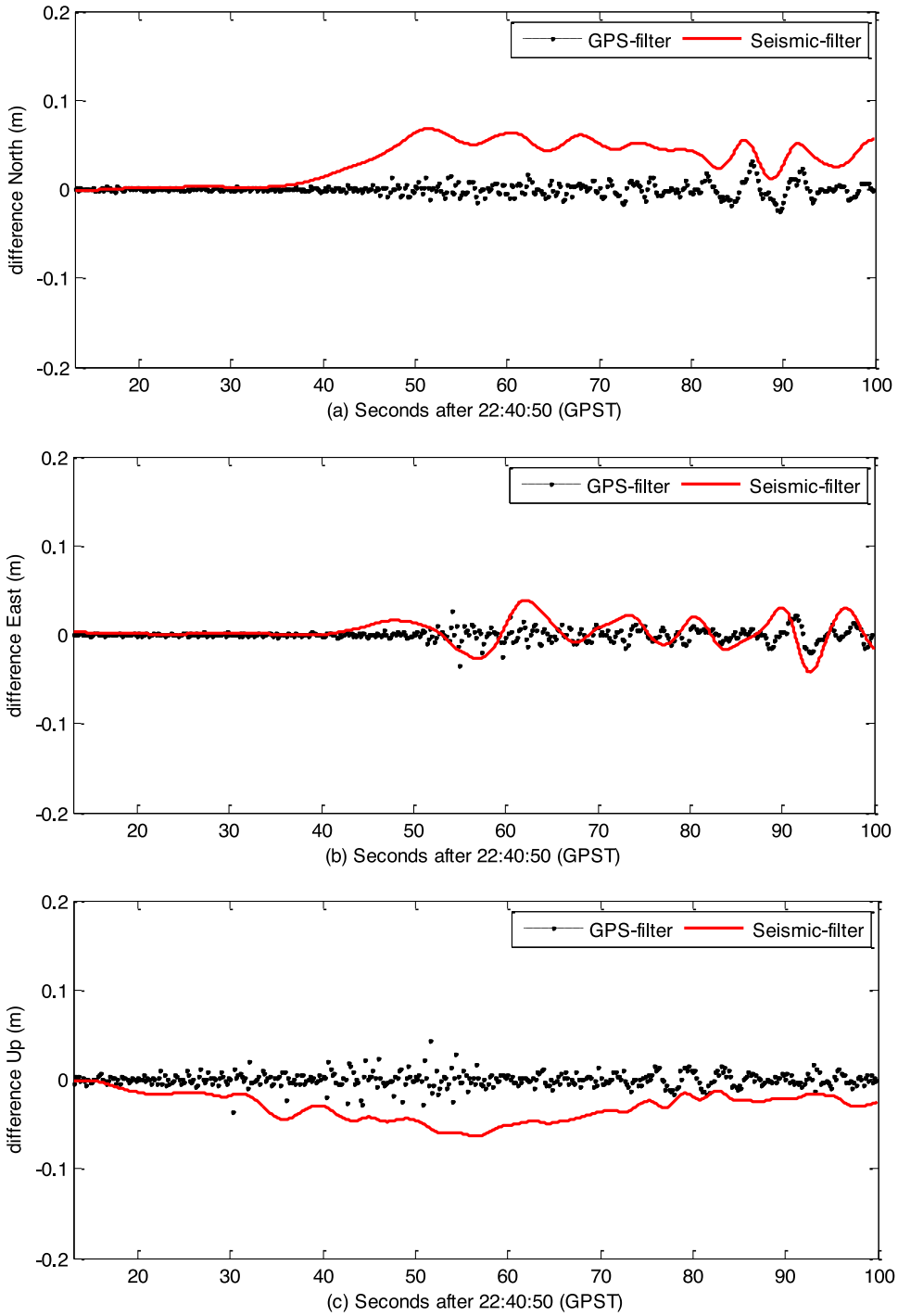

Figure 6. Difference between the displacement series from tightly integrated filter and each of the two inputs (GPS and seismic displacements) for 5060/P499 pair. The differences between GPS-only and filter displacements are shown by the black line, while the differences between seismic-only and filter displacements are shown by the red line. The differences in north, east and up components are, respectively, shown in the subparts (a)–(c).

discriminate between the second set of optimum integer candidates and the optimum one usually with a critical criterion of three (Han 1997).

4 RESULTS

The 2010 M_w 7.2 El Mayor–Cucapah earthquake (2010 April 4, 22:40:42 UTC) in northern Baja California, Mexico, provides us with a real event to evaluate the performance of the proposed tightly integrated approach. GPS data are collected from the California Real-Time Network (CRTN, Genrich & Bock 2006) and Plate Boundary Observatory (PBO, Jackson 2003). 200 Hz accelerometer data are collected from strong motion stations of the Southern California Seismic Network (SCSN) operated by the USGS (U.S. Geological Survey) and Caltech. Table 1 summarizes the station names, locations, distances to epicentre and separations for four collocated stations analysed.

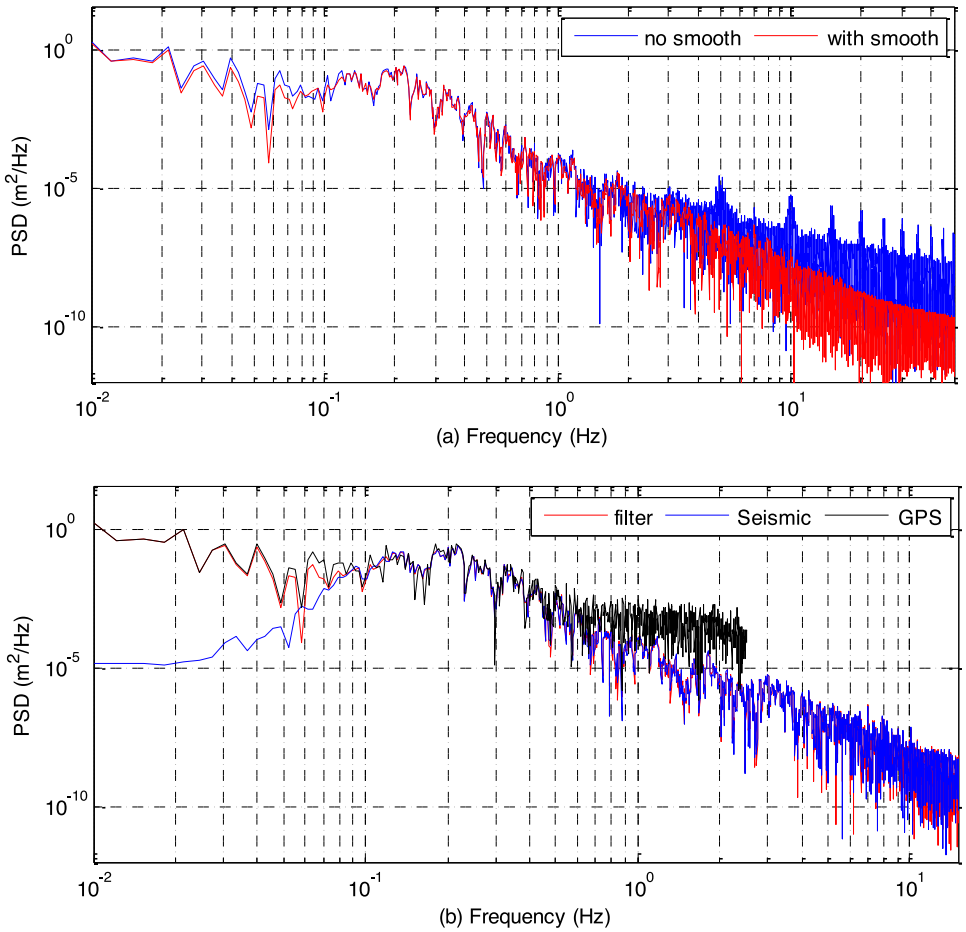

Figure 7. Power spectral densities. (a) Power spectral density for tightly integrated displacement waveforms at P496/5058. The blue line denotes the results without a smoother, while the red line denotes the results with a 5-s lag smoother. (b) Power spectral density for 5 Hz GPS displacements at P496 (the black line), 200 Hz high-pass filtered seismic displacements at 5058 (the blue line) and 200 Hz tightly integrated displacements (with a 5-s lag smoother) at P496/5058 (the red line).

About 90 globally distributed real-time IGS stations are first processed in simulated real-time mode using the EPOS-RT GPS analysis software (Ge *et al.* 2012) for providing orbits, clocks and UPDs at 5-s sampling interval. Based on these corrections, we analyse the collocated high-rate GPS (5 Hz) and accelerometer data (200 Hz).

The proposed tightly integrated algorithm is carried out on a pair-by-pair basis. Displacement waveforms are estimated for each collocated pair of GPS and strong motion sensors using the presented tightly integrated filter, in a simulated real-time mode. We compare the integrated displacements with GPS-only displacements derived from real-time ambiguity-fixed PPP and seismic-only displacements obtained through double integration of seismic accelerations. The seismic-only displacements in this study are provided by California Geological Survey [CGS/CSMIP, http://strongmotioncenter.org/ (last accessed July 2013)]. The baseline offsets are already corrected by applying a high-pass filter.

The GPS station P496, which is located about 60 km from the epicentre, is collocated with SCSN seismic station 5058 (about 140 m distance). Comparison of the GPS-only, seismic-only and tightly integrated displacements in all three components for this pair (5058/P496) is exemplarily shown in Fig. 1 by black, blue and red lines, respectively.

In Fig. 1(a), we show the entire period of seismic shaking in the north component. The GPS-only and seismic-only displacements show a high degree of similarity of the dynamic component. The standard deviation (*SD*) values of the differences between GPS-only and seismic-only displacements are found to be 1.1, 1.0 and 2.1 cm, respectively, in north, east and vertical components. The obvious difference is that a permanent coseismic offset of 0.2 m is visible in the GPS-only displacements. Tilt and rotation of the seismic instrument result in distortions and baseline offsets. Although these effects are largely removed by high-pass filter, low-frequency information is lost, including the loss of permanent coseismic offset in the seismic-only displacements (Allen & Ziv 2011). In the tightly integrated displacements, the 0.2 m permanent offset in the north component is clearly seen as the seismic data are constrained by the long-period stability of GPS measurements and the baseline-shift problem in seismic data can be overcome. The 5 Hz GPS-only displacements are with lower sampling rate and higher noise compared to the 200 Hz seismic-only displacements. The rms values of GPS-only solution (10 min pre-event displacement series) are found to be 1.1, 1.1 and 3.0 cm, respectively, in north, east and vertical components. The vertical component (Fig. 1c) is the noisiest as expected, due to the satellite constellation configuration and the high correlation between zenith tropospheric delays and the

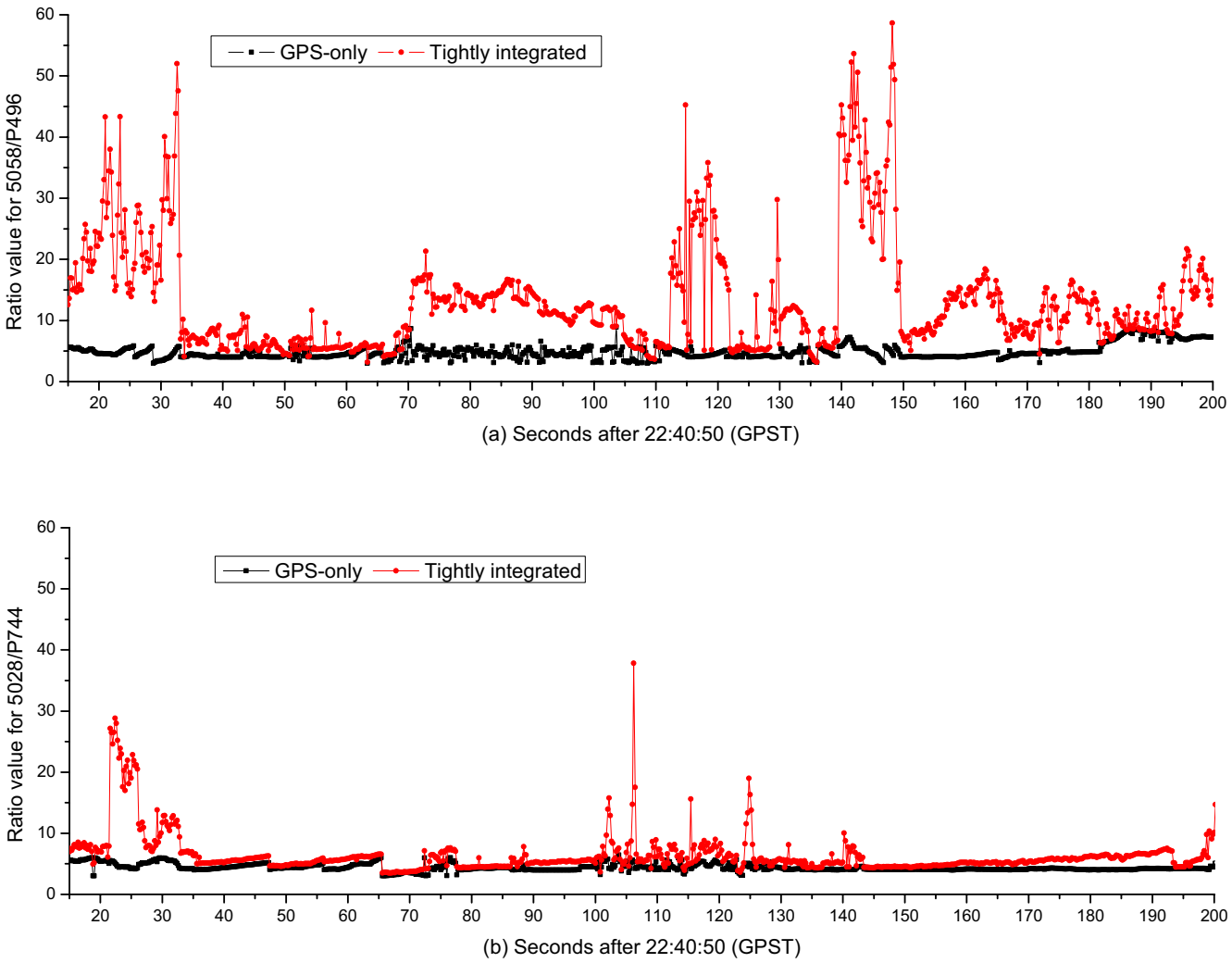

Figure 8. Comparison of the ratio values for tightly integrated and GPS-only solutions: (a) for the collocated 5058 (seismic) and P496 (GPS) pair; (b) for the collocated 5028 (seismic) and P744 (GPS) pair. The ratio values of tightly integrated and GPS-only solutions are shown by the red and black line, respectively.

vertical component. With the aid of the accelerometer data, the tightly integrated filter is capable of producing a more precise waveform. The small-amplitude seismic signal can be detected from the tightly integrated solution (e.g. from 20 to 35 s in Figs 1c and 2c) in spite of the diminished precision of the GPS vertical component. This is a significant improvement compared to the GPS-only solution where earthquake signal is detected only for strong events with significant shaking.

For clarity, the blowup of the displacement series in all three components for its first 45 s is shown in Fig. 2. We can see that the tightly integrated displacements are in good agreement with GPS-only solution in terms of peak displacements and long-period stability. Meanwhile, the displacement precision is also improved by precise dynamical information provided by seismic sensors. The small-amplitude details of the movement (e.g. small shakes around 47 s in Figs 2a–c), which are often covered by measurement noise in GPS-only solution, can be clearly observed from the tightly integrated waveform.

In Fig. 3, we show the differences between tightly integrated filter and GPS-only/seismic-only displacements for the 5058/P496 pair. The results for north, east and up components are, respectively, shown in Figs 3a–c. One can see that the differences between GPS-only and filter displacements show a high-frequency noise due to the diminished precision of the GPS. The differences are more scatter during the strong shaking period. It may be caused by the separation between sensors (not strictly collocated) and/or an overweighting of the accelerometer data in the filter. The differences between seismic-only and filter displacements show a low-frequency trend because of the baseline-shift problem of seismic data. The differenced time-series for the 5028/P744, 5054/P500 and 5060/P499 pairs are shown in Figs 4–6, respectively. Similar performance is also achieved at these pairs, the results confirm that the tight integration of high-rate GPS and very high-rate seismic measurements can take their individual advantages and offset their weakness and improve the displacements significantly.

Power spectral densities for filter displacements at P496/5058 are also shown in Fig. 7(a) to quantify the frequency content of the signal. Similar to Bock *et al.* (2011), a saw tooth pattern in the waveforms associated with the multirate aspect of the filter was shown to have an impact in the power spectra (the blue line). However, it is a minor problem for real-time seismological applications as the increase in noise introduced by the peaks is small compared with

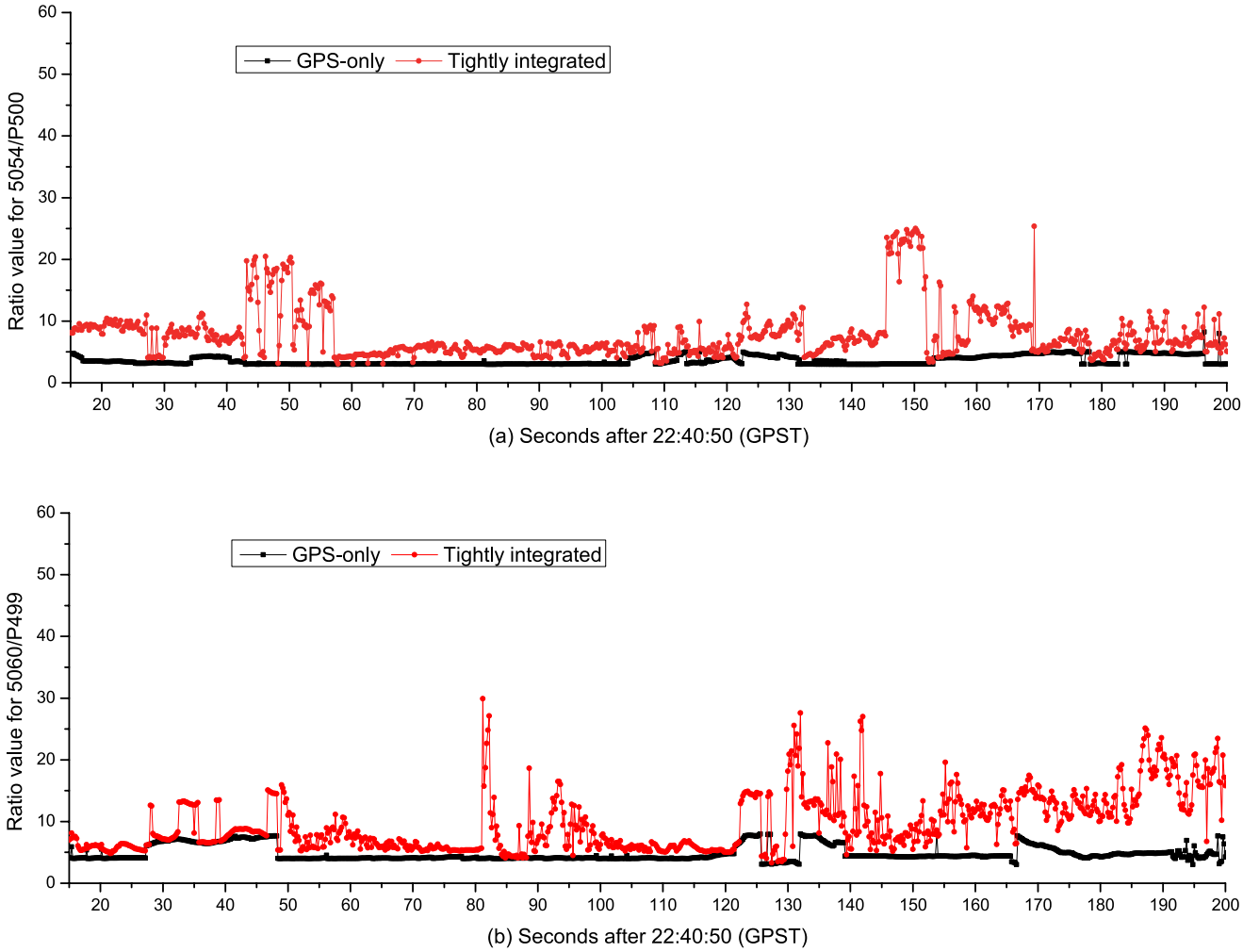

Figure 9. Comparison of the ratio values for tightly integrated and GPS-only solutions: (a) for the collocated 5054 (seismic) and P500 (GPS) pair; (b) for the collocated 5060 (seismic) and P499 (GPS) pair. The ratio values of tightly integrated and GPS-only solutions are shown by the red and black line, respectively.

the signal. Furthermore, the spurious peaks can be removed by a 5-s lag smoother, which is also shown by the red line (Bock *et al.* 2011; Melgar *et al.* 2013). The power spectral densities of the three kinds of displacements (5 Hz GPS, 200 Hz seismic and 200 Hz tightly integrated filter with a 5-s lag smoother) are also compared in Fig. 7(b). The frequency domain analysis of these waveforms describes what frequency bands each data type is reliable in: GPS performs better at the lower frequencies and accelerometer is better at the higher frequencies. The power spectral densities of filter displacements follow the GPS-only spectrum at the low frequencies and the accelerometer-only spectrum at the high frequencies. From the power spectral density analysis, we can also infer that the filter waveform is more precise and accurate than the (5 Hz) GPS-only or (200 Hz) seismic-only waveforms, that is, an accurate broad-band waveform has been achieved.

Fixing ambiguities is a prerequisite to achieve high-accuracy positioning results in GNSS applications. The ratio of the second minimum to the minimum quadratic form of residuals (R-ratio) is used here to decide the correctness and confidence level of integer ambiguity candidate. The ratio value can be considered as an index to denote the reliability of ambiguity resolution. Thus, larger ratio values denote more reliable ambiguity resolution. The ratio values of tightly integrated and GPS-only solution for 5058/P496 and 5028/P744 pairs are, respectively, shown in Figs 8(a) and (b). The ratio values of tightly integrated solution are shown by the red line, while the ratio values of GPS-only solution are shown by the black line. As shown in Fig. 8, the ratio values of GPS-only solution are generally rather small and below 5 usually. With the aid of the accelerometer data, the ratio values are increased remarkably compared to that of GPS-only. The averaged ratio is increased from 4.5 and 3.8 of GPS-only for 5058/P496 and 5028/P744 pairs to 11.6 and 6.4 of the tightly integrated solution, respectively. The results indicate that the proposed algorithm can significantly improve the ability of resolving integer-cycle phase ambiguities, which is very critical for promoting the contribution of GPS phase observations. The comparison of ratio values for 5054/P500 and 5060/P499 pairs are also, respectively, shown in Figs 9(a) and (b). The average values of GPS-only ratio values for these two pairs are improved from about 3.6 and 4.8 to 8.0 and 10.1, respectively.

5 CONCLUSIONS

We presented an approach for tightly combing GPS and seismic sensor data where the accelerometer data are integrated into the

ambiguity-fixed PPP processing on the observation level. The performance of the proposed tightly integrated approach was validated using the collocated high-rate GPS and strong motion data collected during the 2010, M_w 7.2 El Mayor–Cucapah earthquake. For tightly integrated displacements, the peak displacements and long-period stability are in agreement with GPS-only solution. As a typical example, the permanent coseismic offset which is usually underestimated in the seismic-only solution can be now obtained exactly in the integrated solution. Some small-amplitude seismic details, which are not detectable in the GPS-only approach, can be detected from the tightly integrated displacements. A power spectral density analysis also demonstrates that an accurate broad-band displacement waveform can be derived from the tightly integrated filter. Furthermore, the ratio values of the tightly integrated solutions are significantly improved from about four of the GPS-only solutions to 10 on average.

ACKNOWLEDGEMENTS

We would like to thank Prof. Duncan Agnew, Prof. Kristine Larson and an anonymous reviewer for their detailed and constructive comments. The GPS data (5 Hz) used to derive the displacement waveforms were provided by the Plate Boundary Observatory operated by UNAVCO for EarthScope [http://www.earthscope.org (last accessed July 2013)] and supported by NSF grant EAR-0323309. The accelerometer data (200 Hz) were provided by the Southern California Seismic Network (SCSN) operated by the USGS (U.S. Geological Survey) and Caltech. Thanks also to the International GNSS Service (IGS) for providing GPS data of globally distributed reference stations.

REFERENCES

Allen, R. & Ziv, A., 2011. Application of real-time GPS to earthquake early warning, *Geophys. Res. Lett.,* **38**(16), L16310, doi:10.1029/2011GL047947.

Blewitt, G., 1989. Carrier phase ambiguity resolution for the Global Positioning System applied to geodetic baselines up to 2000 km, *J. geophys. Res.,* **94,** 10 187–10 203.

Blewitt, G., Kreemer, C., Hammond, W.C., Plag, H.-P., Stein, S. & Okal, E., 2006. Rapid determination of earthquake magnitude using GPS for tsunami warning systems, *Geophys. Res. Lett.,* **33,** L11309, doi:10.1029/2006GL026145.

Blewitt, G., Hammond, W.C., Kreemer, C., Plag, H.-P., Stein, S. & Okal, E., 2009. GPS for real-time earthquake source determination and tsunami warning systems, *J. Geod.,* **83,** 335–343.

Bock, Y., Nikolaidis, R., de Jonge, P.J. & Bevis, M., 2000. Instantaneous geodetic positioning at medium distances with the global positioning system, *J. geophys. Res.,* **105,** 28 233–28 253.

Bock, Y., Melgar, D. & Crowell, B.W., 2011. Real-time strong-motion broadband displacements from collocated GPS and accelerometers, *Bull. seism. Soc. Am.,* **101**(6), 2904–2925.

Boore, D.M., Stephens, C.D. & Joyner, W.B., 2002. Comments on baseline correction of digital strong-motion data: examples from the 1999 Hector Mine, California, earthquake, *Bull. seism. Soc. Am.,* **92,** 1543–1560.

Chan, W., Xu, Y., Ding, X. & Dai, W., 2006. An integrated GPS-accelerometer data processing technique for structural deformation monitoring, *J. Geod.,* **80**(12), 705–719.

Collins, P., Lahaye, F., Hérous, P. & Bisnath, S., 2008. Precise point positioning with AR using the decoupled clock model, in *Proceedings of ION GNSS 2008,* 16–19 September, GA, USA.

Crowell, B., Bock, Y. & Squibb, M., 2009. Demonstration of earthquake early warning using total displacement waveforms from real time GPS networks, *Seismol. Res. Lett.,* **80,** 772–782.

Crowell, B.W., Bock, Y. & Melgar, D., 2012. Real-time inversion of GPS data for finite fault modeling and rapid hazard assessment, *Geophys. Res. Lett.,* **39,** L09305, doi:10.1029/2012GL051318.

Dong, D.N. & Bock, Y., 1989. Global Positioning System network analysis with phase ambiguity resolution applied to crustal deformation studies in California, *J. geophys. Res.,* **94,** 3949–3966.

Emore, G., Haase, J., Choi, K., Larson, K.M. & Yamagiwa, A., 2007. Recovering seismic displacements through combined use of 1-Hz GPS and strong-motion accelerometers, *Bull. seism. Soc. Am.,* **97,** 357–378.

Ge, L., 1999. GPS seismometer and its signal extraction, in *Proceedings of the 12th International Technical Meeting of the Satellite Division of the Institute of Navigation,* Institute of Navigation, Fairfax, VA, pp. 41–52.

Ge, L. *et al.*, 2000. GPS seismometers with up to 20 Hz sampling rate, *Earth Planets Space,* **52**(10), 881–884.

Ge, M., Gendt, G., Rothacher, M., Shi, C. & Liu, J., 2008. Resolution of GPS carrier-phase ambiguities in precise point positioning (PPP) with daily observations. *J. Geod.,* **82**(7), 389–399.

Ge, M., Dousa, J., Li, X., Ramatschi, M. & Wickert, J., 2012. A novel real-time precise positioning service system: global precise point positioning with regional augmentation, *J. Global Position. Syst.,* **11**(1), 2–10.

Geng, J., Meng, X., Dodson, A., Ge, M. & Teferle, F., 2010. Rapid re-convergences to ambiguity-fixed solutions in precise point positioning, *J. Geod.,* **84,** 705–714.

Geng, J., Shi, C., Ge, M., Dodson, A.H., Lou, Y., Zhao, Q. & Liu, J., 2012. Improving the estimation of fractional-cycle biases for ambiguity resolution in precise point positioning, *J. Geod.,* **86,** 579–589.

Geng, J., Bock, Y., Melgar, D., Crowell, B.W. & Haase, J., 2013, A new seismogeodetic approach applied to GPS and accelerometer observations of the 2012 Brawley seismic swarm: implications for earthquake early warning, *Geochem. Geophys. Geosyst.,* doi:10.1002/ggge.20144.

Genrich, J.F. & Bock, Y., 2006. Instantaneous geodetic positioning with 10–50 Hz GPS measurements: noise characteristics and implications for monitoring networks, *J. geophys. Res.,* **111,** doi:10.1029/2005JB003617.

Han, S., 1997. Quality-control issues relating to instantaneous ambiguity resolution for real-time GPS kinematic positioning. *J. Geod.,* **71**(6), 351–361.

Hirahara, K., Nakano, T. & Hoso, Y., 1994. An experiment for GPS strain seismometer, in *Proceedings of the Japanese Symposium on GPS,* 15–16 December, Tokyo, Japan, pp. 67–75.

Jackson, M., 2003. Geophysics at the speed of light: earthscope and the plate boundary observatory, *Leading Edge,* **22,** 262–267.

Kogan, M.G., Kim, W.Y., Bock, Y. & Smyth, A.W., 2008. Load response on the Verrazano Narrows Bridge during the NYC Marathon revealed by GPS and accelerometers, *Seismol. Res. Lett.,* **79,** 12–19.

Kouba, J., 2003. Measuring seismic waves induced by large earthquakes with GPS, *Stud. Geophys. Geod.,* **47,** 741–755.

Kouba, J & Héroux, P., 2001. Precise point positioning using IGS orbit and clock products. *GPS Solut.,* **5**(2), 12–28.

Larson, K., 2009. GPS seismology, *J. Geod.,* **83,** 227–233.

Larson, K., Bodin, P. & Gomberg, J., 2003. Using 1-Hz GPS data to measure deformations caused by the Denali fault earthquake, *Science,* **300,** 1421–1424.

Laurichesse, D., Mercier, F., Berthias, J.P. & Bijac, J., 2008. Real time zero-difference ambiguities fixing and absolute RTK, in *Proceedings of ION National Technical Meeting,* 28–30 January, San Diego, CA, USA.

Lee, V.W. & Trifunac, M.D., 2009. Empirical scaling of rotational spectra of strong earthquake ground motion, *Bull. seism. Soc. Am.,* **99,** 1378–1390.

Li, T. & Wang, J., 2012. Some remarks on GNSS integer ambiguity validation methods, *Survey Rev.,* **44**(326), 320–328.

Li, X & Zhang, X., 2012. Improving the estimation of uncalibrated fractional phase offsets for PPP ambiguity resolution, *J. Navig.,* **65,** 513–529.

Li, X., Ge, M., Zhang, X., Zhang, Y., Guo, B., Wang, R., Klotz, J. & Wickert, J., 2013a. Real-time high-rate co-seismic displacement from ambiguity-fixed precise point positioning: application to earthquake early warning, *Geophys. Res. Lett.,* **40,** 295–300.

Li, X., Ge, M., Zhang, H. & Wickert, J., 2013b. A method for improving uncalibrated phase delay estimation and ambiguity-fixing in real-time precise point positioning. *J. Geod.,* **87,** 405–416.

Loyer, S., Perosanz, F., Mercier, F., Capdeville, H. & Marty, J., 2012. Zero-difference GPS ambiguity resolution at CNES-CLS IGS analysis center, *J. Geod.,* **86,** 991–1003.

Melgar, D., Bock, Y. & Crowell, B.W., 2012. Real-time centroid moment tensor determination for large earthquakes from local and regional displacement records, *Geophys. J. Int.,* **188,** 703–718.

Melgar, D., Bock, Y., Sanchez, D. & Crowell, B.W., 2013, On robust and reliable automated baseline corrections for strong motion seismology, *J. geophys. Res. Solid Earth,* **118,** 1177–1187.

Nikolaidis, R, Bock, Y., de Jonge, P.J., Shearer, P., Agnew, D.C. & Van Domselaar, M., 2001. Seismic wave observations with the Global Positioning System, *J. geophys. Res.,* **106,** 21 897–21 916.

Ohta, Y. *et al.*, 2012. Quasi real-time fault model estimation for near-field tsunami forecasting based on RTK-GPS analysis: application to the 2011 Tohoku-Oki earthquake (Mw 9.0), *J. geophys. Res.,* **117**(B2), B02311, doi:10.1029/2011JB008750.

Remondi, B., 1985. Performing centimeter-level surveys in seconds with GPS carrier phase: initial results, *Navigation,* **32,** 386–400.

Schaffrin, B. & Bock, Y., 1988. A unified scheme for processing GPS dual-band phase observations, *Bull. Geod.,* **62,** 142–160.

Smyth, A. & Wu, M., 2006. Multi-rate Kalman filtering for the data fusion of displacement and acceleration response measurements in dynamic system monitoring, *Mech. Syst. Signal Process.,* **21,** 706–723.

Teunissen, P.J.G., 1995. The least squares ambiguity decorrelation adjustment: a method for fast GPS integer estimation, *J. Geodesy,* **70,** 65–82.

Teunissen, P.J.G. & Kleusberg, A., 1996. *GPS for Geodesy, Volume 60 of Lecture Notes in Earth Sciences,* pp. 175–217, Springer-Verlag.

Trifunac, M.D. & Todorovska, M.I., 2001. A note on the usable dynamic-crange of accelerographs recording translation, *Soil Dyn. Earthq. Eng.,* **21,** 275–286.

Wang, R., Parolai, S., Ge, M., Ji, M., Walter, T.R. & Zschau, J., 2013. The 2011 Mw 9.0 Tohoku-Oki earthquake: comparison of GPS and strong-motion data, *Bull. seism. Soc. Am.,* **103**(2B), 1336–1347.

Wright, T.J., Houlié, N., Hildyard, M. & Iwabuchi, T., 2012. Real-time, reliable magnitudes for large earthquakes from 1 Hz GPS precise point positioning: the 2011 Tohoku-Oki (Japan) earthquake, *Geophys. Res. Lett.,* **39,** L12302, doi:10.1029/2012GL051894.

Zhang, X. & Li, X., 2012. Instantaneous re-initialization in real-time kinematic PPP with cycle-slips fixing, *GPS Solut.,* **16,** 315–327.

Zumberge, J.F., Heflin, M.B., Jefferson, D.C., Watkins, M.M. & Webb, F.H., 1997. Precise point positioning for the efficient and robust analysis of GPS data from large networks, *J. geophys. Res.,* **102**(B3), 5005–5017.